CHEMIJA. 2004. T. 15. Nr. 3. P. 17–25

Corrosion of Zn and Zn alloy electrodeposits: morphology and structural changes

Algirdas Selskis[1], Laima Gudavičiūtė[1], Ignas Valsiūnas[1], Rimantas Ramanauskas[2*]

[1] *Institute of Chemistry, A. Goštauto 9, LT-01108 Vilnius, Lithuania*
[2] *Vilnius Pedagogical University, Studentų 39, LT-08106 Vilnius, Lithuania*

The corrosion behaviour of electrodeposited Zn, Zn–Co(0.6%), Zn–Fe(0.4%) and Zn–Ni(12%) coatings in a HCO_3^--containing NaCl solution was investigated. The corrosion rates and the oxide films formed were analyzed in relation to coating microstructure. The atomic force microscopy (AFM) technique was applied to study the surface morphology and to estimate the roughness parameters, while X-ray diffraction (XRD) was used to observe changes in the sample texture after a corrosion attack and to evaluate lattice distortions. It has been assumed that the oxide film plays a significant role in this process. A higher corrosion resistance of Zn–Co and Zn–Ni coatings may be related to the fact that bare surfaces of these samples are more active because of a higher number of lattice imperfections. Such structural peculiarities lead to a faster oxide film formation with the properties that result in a reduction of the coating corrosion rate. The corrosion process of the alloys was observed to be more uniform, while local corrosion attack was more pronounced for pure Zn surface.

Key words: Zn and Zn alloys, electrodeposits, corrosion, structure

INTRODUCTION

Zn co-deposition with Fe group metals enhances notably coating corrosion resistance. Certain differences between Zn and Zn–Co, Zn–Fe and Zn–Ni electrodeposit corrosion behaviour in natural atmospheric conditions and some aqueous solutions have been reported [1–3]. Fundamental studies on Zn corrosion are extensive and have been recently summarized by Zhang [4], however, most of them provide a macroscopic view of the process. Perhaps due to this, the nature of the corrosion inhibition phenomenon by alloying is not yet fully understood.

Metal dissolution is known to occur mainly at surface active sites where atoms are weakly bonded to crystal surface. The number of such active sites and hence their relative importance in relation to corrosion reaction rate is dependent on the surface texture (nm level) and surface topography (10–100 nm level) [5]. The influence of structural parameters is more pronounced when corrosion occurs under conditions of active (film-free) dissolution. Meanwhile, the differences in corrosion behaviour between the coatings studied manifest exclusively under the conditions when a passivating corrosion product, film, forms on the sample surface [3]. A recent study [6] on the anodically formed oxide films on the same coatings has shown that alloy composition can affect the thickness, constitution, crystallinity and defective structure of the obtained passive layers. It was assumed here that oxide film properties depend heavily on metal structural parameters.

In general, the use of a number of techniques is required to obtain a complete view of the corrosion process. Atomic force microscopy (AFM) and X-ray diffraction (XRD) with grazing incidence geometry are receiving considerable attention due to their ability to provide microscopic information. As AFM can image the insulating layers, it is therefore appropriate for corrosion studies providing information on the corroding metal surface morphology changes. XRD with grazing incidence geometry enables us to obtain information on the coating texture, lattice parameters and defects from the superficial layers [1].

The present investigation was aimed to find evidences on a link between Zn, Zn–Co, Zn–Fe and Zn–Ni electrodeposit morphology, crystallographic orientation, lattice imperfection and their corrosion behaviour in a HCO_3^--ion containing NaCl solution.

EXPERIMENTAL

Zn, Zn–Co (0.6%), Zn–Fe (0.4%) and Zn–Ni (12%) coatings 10 μm thick were electrodeposited on low carbon steel samples, which had been previously po-

* Corresponding author. ramanr@ktl.mii.lt

lished mechanically to a bright mirror finish using the 0.3 μm alumina powder for the final step. The plating bath compositions and operating conditions are given in [1–3]. The prepared samples were immersed in a solution containing 0.6 M NaCl and 0.2 M $NaHCO_3$ (pH 6.8) and then were analyzed first by the XRD and then AFM techniques after different immersion periods. An additional set of samples was prepared for the electrochemical measurements.

XRD measurements were carried out with a Siemens diffractometer with a grazing incidence geometry (model D 5000), Cu monochromatic radiation λ = 1.5418 Å (35 mA and 40 kV), with a 0.01° step and 4.8 s per step counter time, applying 1° and 10° X-ray beam incidence angle. The quantitative method for determining the degree of crystallographic texture was applied [7].

AFM studies were carried out with an AFM AutoProbe CP (Park Scientific Instruments) at atmospheric pressure and room temperature in a contact mode. Three images of distinct size were taken in different location sites of each sample in *ex-situ* conditions. The same applied force and the same conditions into the feedback loop were used to ensure reproducibility. AFM images were obtained with the same micro-lever, thus the obtained root-mean-squared roughness (R_{rms}) and peak-to-valley distance ($R_{p\text{-}v}$) parameters can be compared for different samples.

All the electrochemical measurements were performed using a standard three-electrode system with a Pt counter electrode, a saturated calomel reference electrode and a GAMRY CMS/100 corrosion measuring system. For the corrosion tests, the working electrodes were introduced into the cell immediately after electroplating.

The oxide film from the coating surface after a corrosion attack was removed by immersing the sample for 10 s in a saturated ammonium acetate solution, followed by ultrasonic cleaning in distilled water.

RESULTS AND DISCUSSION

Corrosion measurements

Zn corrosion in near neutral, uncomplexing solutions occurs with oxide/hydroxide film formation. In unbuffered Cl^- media this film is somewhat porous and therefore not of passivating type, while in a HCO_3^--containing Cl^- solution the oxide film is supposed to be more compact, adherent and less soluble, thus exhibiting a passivating character [8]. According to our investigations [9], the results of aqueous corrosion of Zn and Zn alloy coatings in a HCO_3^--containing NaCl solution were detected to be in general agreement with that obtained under atmospheric conditions. Therefore, this medium was considered to be suitable for studying the Zn and Zn alloy corrosion process.

The specimen corrosion current densities (i_{corr}) were determined from polarization resistance measurements for the different sample immersion periods (Fig. 1a). The Tafel slope values obtained previously [9] were applied. Zn–Fe and Zn coatings starting from the first hours of immersion show higher corrosion rates with respect to the other two alloys. Besides, their i_{corr} values tend to maintain constant values when the immersion time exceeds 8 h (~$5 \cdot 10^{-5}$ A cm^{-2}). While, Zn–Ni and Zn–Co samples show significantly lower i_{corr} values (1–2 · · 10^{-5} A cm^{-2}).

Both zinc oxide and zinc hydroxide are common Zn corrosion products in dilute NaCl solutions, the latter being formed in various amounts as a minor component [4]. The amount of oxide which forms on the coating surface during its corrosion was determined from the cathodic polarization measurements. The oxide phase reduction peak was integrated after the baseline was created, and the charge (Q_c) consumed for this process was evaluated. Figure 1b shows the variations in the Q_c value for different sample immersion times. It is evident that the corrosion product, film, is thinner for coatings that show lower i_{corr} values (Zn–Co and Zn–Ni). During the initial corrosion period (approximately

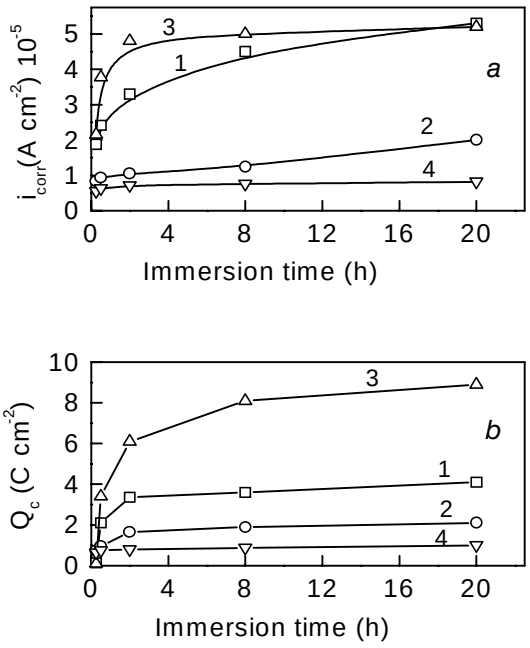

Fig. 1. Corrosion current (*a*) and charge consumed for oxide film reduction (*b*) of Zn and Zn alloy samples immersed in HCO_3^- + NaCl solution: *1* – Zn, *2* – Zn–Co, *3* – Zn–Fe, *4* – Zn–Ni

15 min) the Q_c values are higher for Zn–Co and Zn–Ni electrodes (0.6–0.7 · 10^{-5} C) than for the Zn and Zn–Fe ones (0.1–0.14 · 10^{-5} C). Although, after 30 min of sample immersion, the film is thicker on the latter group of samples.

We can state therefore that oxide film growth rates on Zn and Zn alloy surfaces and their corrosion protection properties depend on the nature of the coating. Lower corrosion rates are accompanied by thinner oxide film formation.

AFM studies

The surface of Zn and Zn alloy coatings before and after different periods of corrosion attack were examined. The images characteristic of every sample are shown in Figs. 2–5.

After electrodeposition Zn, Zn–Co and Zn–Fe coating surfaces appeared to be fine-grained with pyramidal-shaped crystals (Figs. 2a–4a). For Zn and Zn–Co samples the crystal diameter ranged between 25–75 nm, meanwhile for Zn–Fe it varied within 50 to 100 nm. Furthermore, all these coatings were bright, except Zn–Ni whose surface was dull in appearance. The terrace stepped structure was observed for the Zn–Ni sample. It possessed a nodular fine-grained morphology (Fig. 5a), with the grain size in the order of 1–2 μm. At the same time, the surface of this alloy was rougher in comparison with the other three coatings.

Due to the stochastic nature of the metal corrosion process the surface morphology is expected to change with time [5, 10]. Surface morphology evolution during sample immersion in an HCO_3^--containing NaCl solution was examined by *ex situ* AFM studies. The obtained images are presented in Figs. 2–5b, c, d.

Oxide phase formation is the very first stage of Zn corrosion in a nearly neutral solution. Some grain boundary locations, which are sites of active metal dissolution, can be observed, especially on a pure Zn sample (Fig. 2b), in spite of the presence of oxide layer on the corroded samples. However, the oxide phase caused difficulties in a detailed analysis of the underlayer crystal microstructure.

In order to obtain information on the coating morphology modification during a surface corrosion attack, the oxide overlayer was removed with an ammonium acetate solution. Only the oxide phase was dissolved during this procedure, revealing the surface structure of the corroded coating. AFM images of such surfaces are presented in Figs. 2–5c, d.

Changes in surface morphology during the corrosion of coatings appeared to be dependent on their composition. Variations of the coating surface topography parameters during corrosion attack are pre-

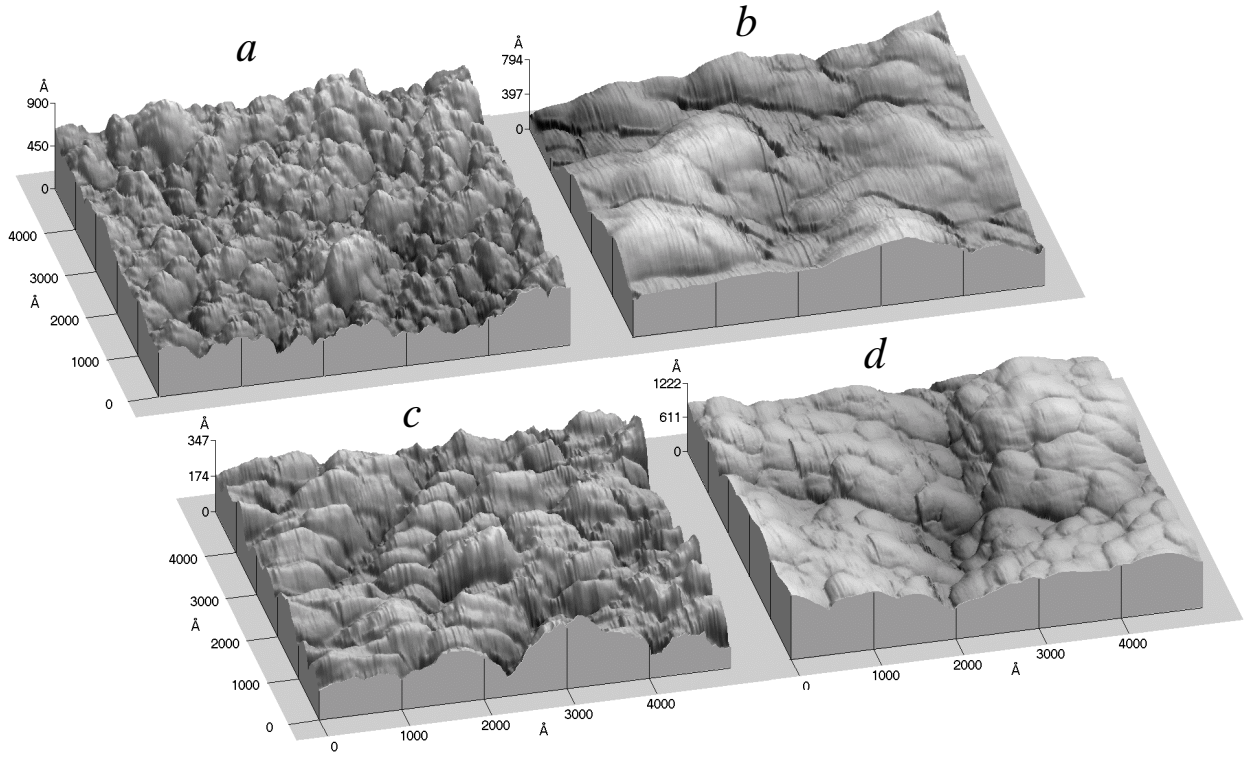

Fig. 2. AFM images of Zn surface: *a* – initial after electrodeposition, *b* – after 0.5 h of corrosion attack with corrosion products, *c* – after 0.5 h of corrosion attack without corrosion products, *d* – after 8 h of corrosion attack, without corrosion products

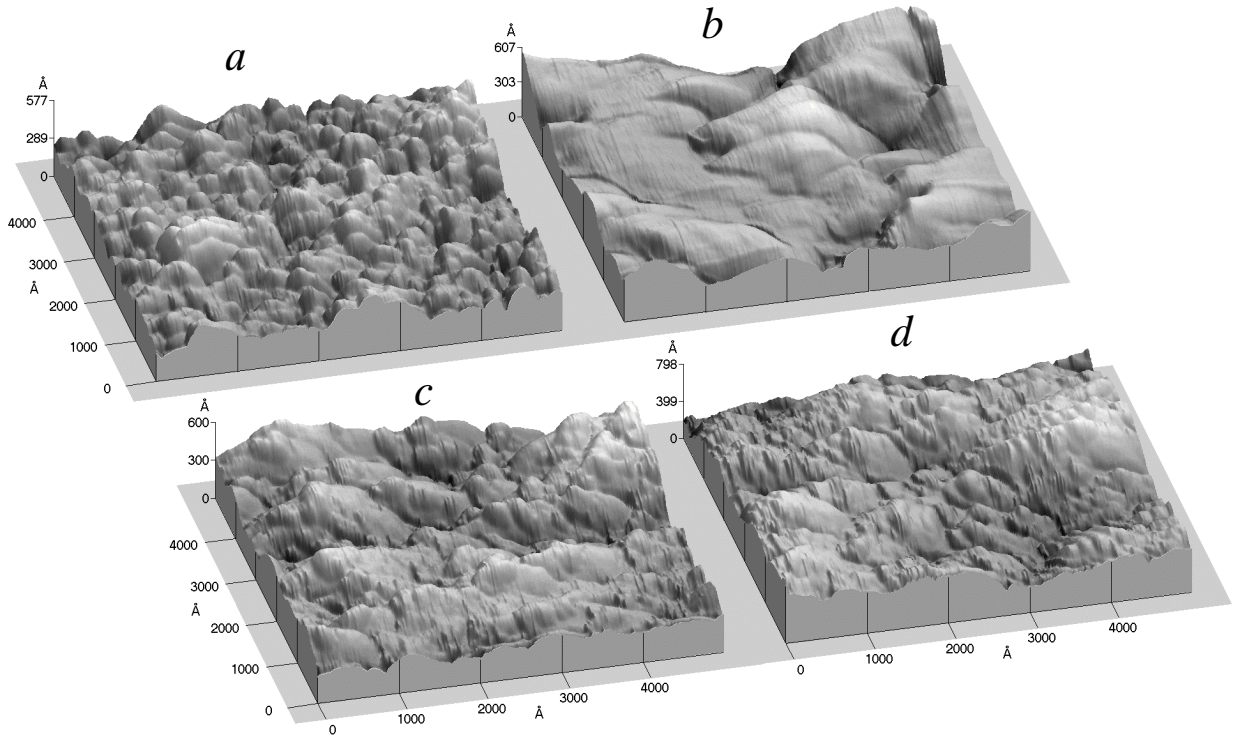

Fig. 3. AFM images of Zn–Co surface: *a* – initial after electrodeposition, *b* – after 0.5 h of corrosion attack with corrosion products, *c* – after 0.5 h of corrosion attack without corrosion products, *d* – after 8 h of corrosion attack, without corrosion products

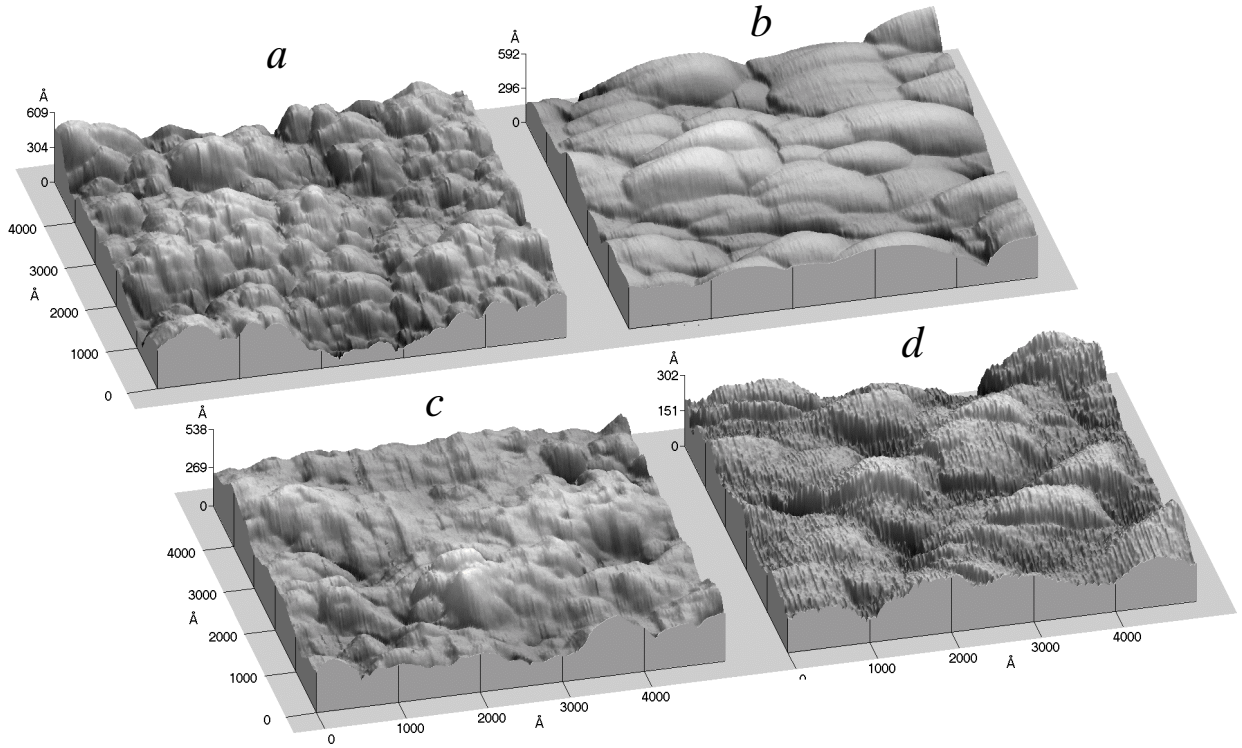

Fig. 4. AFM images of Zn–Fe surface: *a* – initial after electrodeposition, *b* – after 0.5 h of corrosion attack with corrosion products, *c* – after 0.5 h of corrosion attack without corrosion products, *d* – after 8 h of corrosion attack, without corrosion products

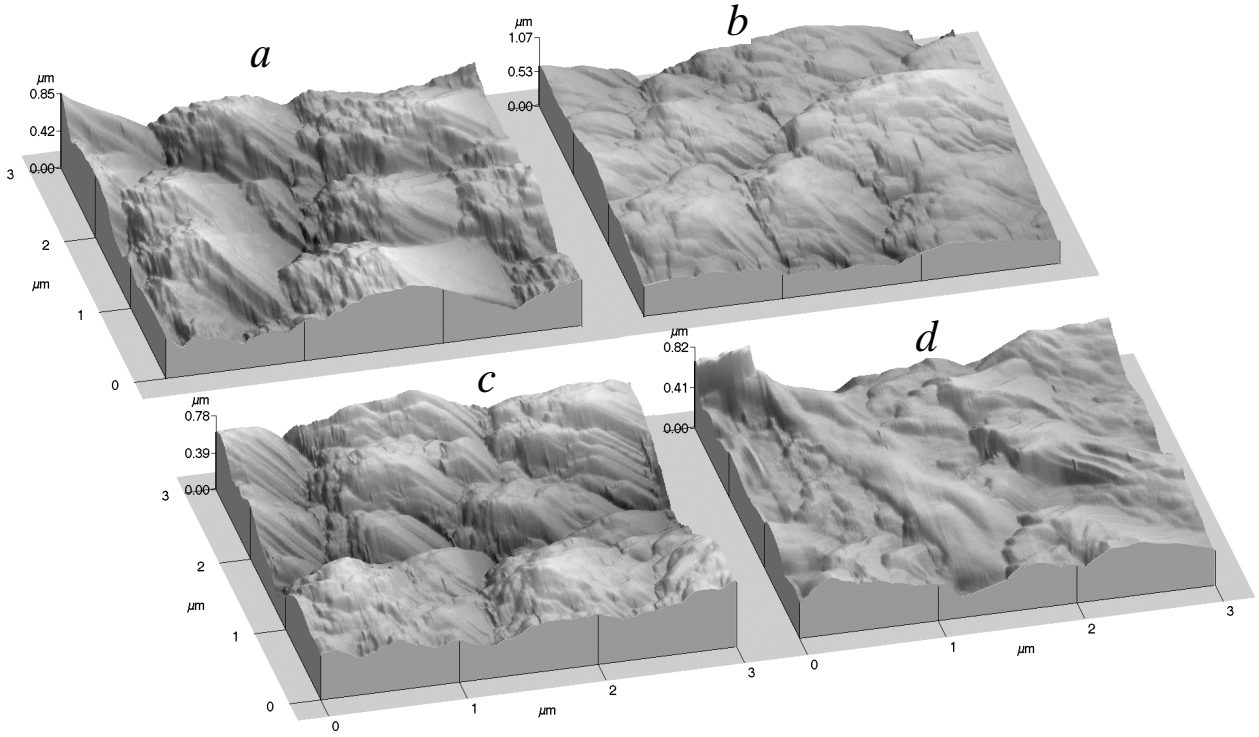

Fig. 5. AFM images of Zn–Ni surface: *a* – initial after electrodeposition, *b* – after 0.5 h of corrosion attack with corrosion products, *c* – after 0.5 h of corrosion attack without corrosion products, *d* – after 8 h of corrosion attack, without corrosion products

sented in Fig. 6. For the initial Zn–Ni surface, 78 nm and 468 nm values of R_{rms} and $R_{p\text{-}v}$ respectively were detected, meanwhile for pure and low-alloyed Zn

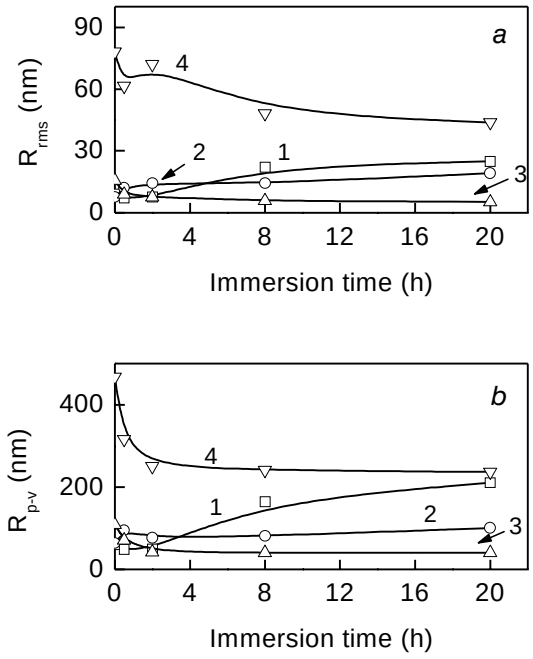

Fig. 6. Morphological parameters R_{rms} (a) and $R_{p\text{-}v}$ (b) changes during Zn and Zn alloy corrosion in HCO_3^- + + NaCl solution (samples without corrosion product film): *1* – Zn, *2* – Zn–Co, *3* – Zn–Fe, *4* – Zn–Ni

these parameters varied between 7–16 nm and 60–100 nm, respectively. A pronounced local corrosion attack took place along some grain boundaries for unalloyed Zn coatings (Fig. 2d). Sample surface roughness increased due to this damage, what coincided with a significant increase in the $R_{p\text{-}v}$ value as compared with that of the initial state (Fig. 6b). Crystal shape changes during Zn coating corrosion took place at the same time as well. They lost their well defined pyramidal shape, became flatter and larger, reaching approximately 50–150 nm in diameter (Fig. 2c, d).

The corrosion process of alloyed coatings regarding surface topography modifications was more uniform. The grain boundaries of Zn–Co alloy were also attacked during sample immersion in the test media (Fig. 3c, d). However, for the alloyed samples this type of damage was less pronounced than for pure Zn. The loss of pyramidal shape took place during Zn alloy corrosion similarly to pure Zn crystals. The most significant changes of surface roughness were detected during the first hour of corrosion attack. An increase in R_{rms} and $R_{p\text{-}v}$ values during the initial period of alloy immersion (up to 0.5 h of treatment) was observed, with the following stabilization of their values.

Zn–Fe and Zn–Ni coating corrosion was accompanied by surface smoothening. For example, a Zn–Fe sample after 2 h of corrosion attack possessed

the lowest R_{rms} and $R_{p\text{-}v}$ values among all the coatings. With an increase in sample immersion time, Zn–Fe crystals lost their pyramidal shape, and flat terrace regions separated by less defined grain boundaries appeared (Fig. 4c), implying that the Zn–Fe alloy corrosion process approached a layer by layer dissolution mechanism.

Some damages along the crystal boundaries for Zn–Ni coatings were present after corrosion attack (Fig. 5c). Nevertheless, R_{rms} and $R_{p\text{-}v}$ values indicate that these changes did not cause surface roughening, *i.e*. Zn–Ni coating corrosion occurred along with the most significant surface smoothening (Fig. 5d).

The development of Zn and Zn alloy surface morphology during their corrosion in HCO_3^- containing NaCl solution implies that the coating microstructure as well as the properties of the formed oxide film may influence the corrosion process rate.

Coating texture

Zn coatings may be electrodeposited with a preferred orientation; furthermore, small amounts of other metal ions in the electrolyte significantly affect the crystal texture [11, 12]. Metal dissolution is known to occur mainly at surface active sites where atoms are weakly bonded to the crystal. Metal atom local coordination is related to planar packing densities, meanwhile the activation energy for dissolution was suggested to increase as the packing density increases [13–15]. Consequently, the crystal orientation factor is supposed to be an important factor in the corrosion process.

Therefore the coating texture before and after corrosion attack was studied. The low incidence angle applied gives information regarding the superficial layers. The XRD patterns of Zn and Zn alloy samples are shown in Figs. 7–10.

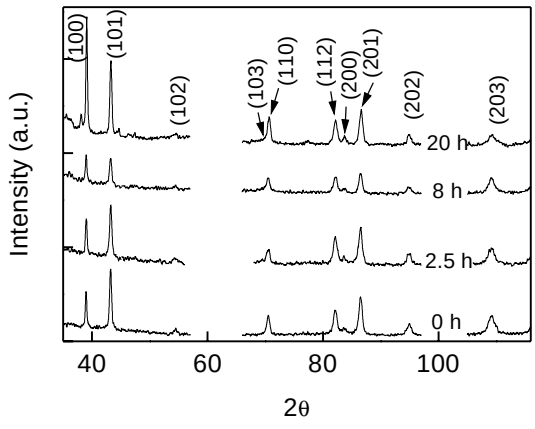

Fig. 7. XRD patterns of Zn coating after different periods of sample immersion in HCO_3^--containing NaCl solution

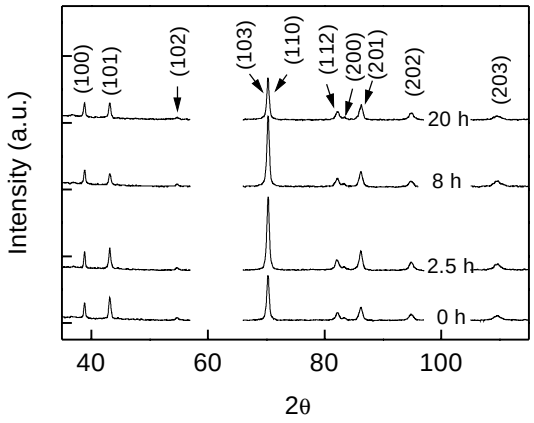

Fig. 8. XRD patterns of Zn–Co coating after different periods of sample immersion in HCO_3^--containing NaCl solution

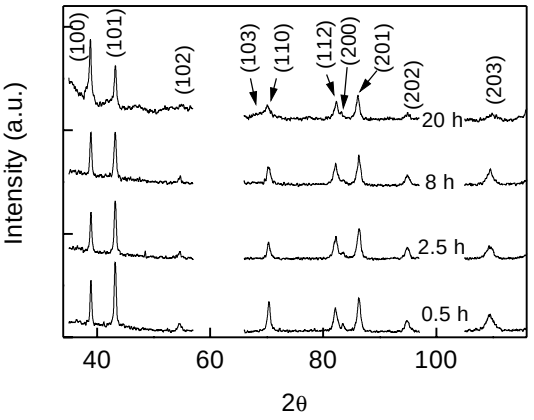

Fig. 9. XRD patterns of Zn–Fe coating after different periods of sample immersion in HCO_3^--containing NaCl solution

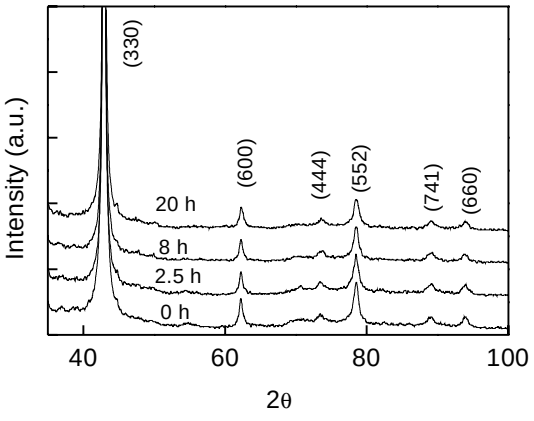

Fig. 10. XRD patterns of Zn–Ni coating after different periods of sample immersion in HCO_3^--containing NaCl solution

Pure Zn and low-alloyed coatings with Co and Fe electrocrystallize with a distorted form of hexagonal close packing. According to the calculated re-

lative texture coefficient (RTC) values presented in Fig. 11 a–d, these coatings had a similar texture. The main difference in their texture was that Zn–Co coatings possessed a higher amount of crystallites with (110) orientation (13%), meanwhile for Zn and Zn–Fe it varied between 3–5%. The packing density of Zn decreased in the order ρ(001) > > ρ(110) > ρ(100) [16]. Thus, crystal texture may be one of the reasons why Zn–Co coatings exhibited a higher corrosion resistance as compared to Zn and Zn–Fe samples.

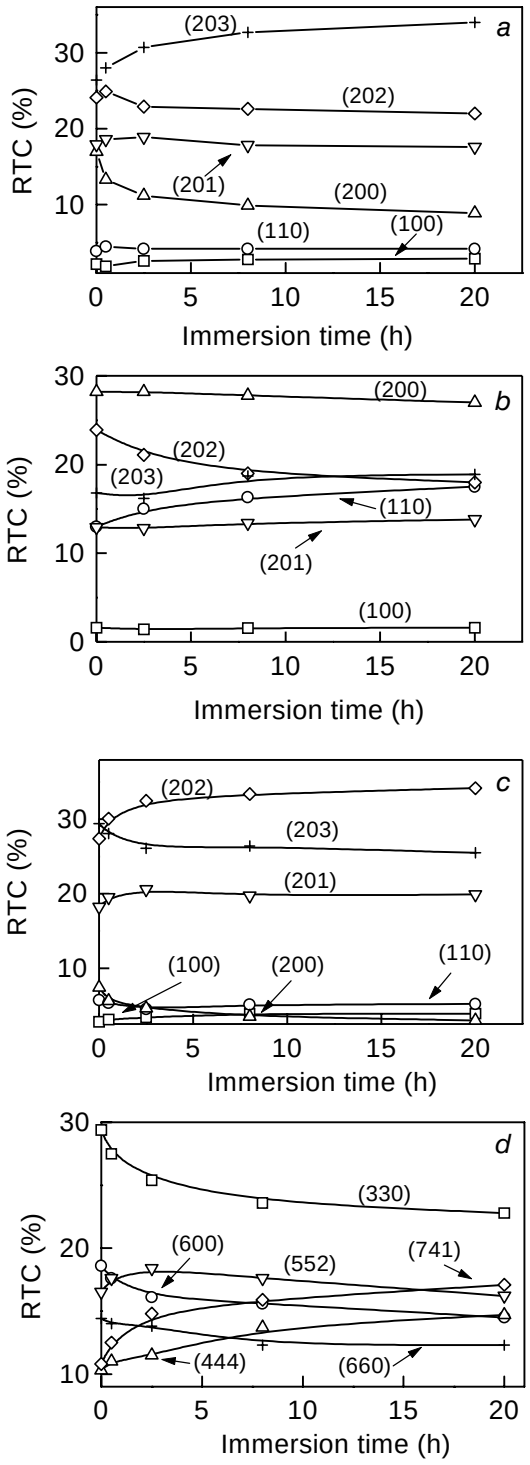

Fig. 11. Relative texture coefficient (RTC) for Zn (*a*), Zn–Co (*b*), Zn–Fe (*c*) and Zn–Ni (*d*) coatings after different periods of sample immersion in HCO_3^--containing NaCl solution

According to XRD data (Fig. 10), Zn–Ni coatings consisted of γ-$Zn_{21}Ni_5$ phase and had a body-centered cubic crystal structure. Approximately 43% of this sample crystallites were oriented parallel to (110) and 18% parallel to (100) planes, implying that these coatings possessed a low-index plane texture.

There was no any additional reflection on the diffractograms of the corroded samples, in spite of the evidence, obtained by electrochemical measurements, that zinc oxide phase had been formed the while corrosion process occurred. This is most probably related to the fact that Zn oxide which forms on investigated surfaces is of amorphous structure [6].

Some XRD reflections of Zn and low-alloyed Zn–Co and Zn–Fe coatings showed a tendency to reduce their intensities, *e.g.*, reflection (200) for all mentioned samples and (202) for Zn and Zn–Co. The reflections whose intensities diminished with increasing corrosion attack time became at the same time broader. Meanwhile, the (110) and (100) reflections did not change significantly their shape or intensity.

The calculated RTC (*hkl*) values (Fig. 11 a–d) corroborate the above-mentioned observations. The main variations of RTC for Zn, Zn–Co and Zn–Fe coatings occurred exactly for crystallites with (20*l*) orientation. The RTC (200) values decreased during their corrosion. The same trend was observed for RTC (202) values of Zn and Zn–Co samples and (203) for Zn–Fe. Meanwhile, the RTC (203) values for Zn, Zn–Co, and (202) for Zn–Fe samples increased with prolonged immersion times. A slight increase in RTC (110) was observed during Zn–Co coating corrosion.

The corrosion of Zn–Ni samples did not cause any variations in the XRD reflection shape (Fig. 10). Nevertheless, their intensity variation induced RTC (*hkl*) changes. The increase in RTC values for the planes with (111) and (741) orientation could be noticed. Meanwhile, the RTC values of (110) and (100) planes decreased with the corrosion process time (Fig. 11 d).

In general, during the corrosion process of Zn and Zn alloy coatings in a HCO_3^- containing NaCl solution, surface morphology changes are more evident than surface texture modifications. Nevertheless, it can be assumed that the prevalence of crystallites with the low-index plane (with a higher packing density) orientation in Zn–Ni and Zn–Co coatings may

be one of the reasons for their higher corrosion resistance. Furthermore, it is known [17] that the growth of Zn oxide film on Zn surface depends on the index of a specific plane. The basal plane is observed to form a thin oxide which has been found to be quite protective, whereas the other planes form thicker films which are less protective. Thus, the Zn coating texture can have a dual effect on its corrosion rate. Therefore, coatings that possess a low-index plane texture are more stable both due to a higher metal atom coordination and the fact that oxide films on such surfaces are more resistant.

Crystal imperfections

The corrosion process is essentially a surface phenomenon, thus it might be strongly related to crystalline perfection. Because of the highly stepped metal surfaces, since the presence of dislocations makes the steps indestructible, it is reasonable to argue that dislocations must be important in the corrosion process.

The X-ray diffraction line broadening is recognized to be caused by crystallite size and lattice strains [18–20]. In general, the grain size of Zn electrodeposits lies in the range 0.1–10 μm, for which X-ray diffraction is quite insensitive to its variation [21, 22], so the observed line broadening will be affected mostly by lattice imperfections. X-ray diffraction measurements were held with a higher beam inclination of 10°, in order to obtain information from the deeper layers. The values of the integral breadth of the different diffraction lines of Zn and low-alloyed coatings are listed in Table 1, and those of Zn–Ni in Table 2.

The introduction of the alloying metal into the Zn matrix increased the integral breadth for all diffraction lines of low-alloyed Zn–Co and Zn–Fe samples. Besides, the Zn–Co sample showed the highest values for almost all reflections, except the (101), implying that the latter coating possessed a more distorted lattice than those of Zn and Zn–Fe alloy.

Table 1. **Integral breadth (10° inclination beam) of Zn and low-alloyed Zn coating diffraction lines**

(*hkl*)	2θ	Integralbreadth (rad) sample		
		Zn	Zn–Co	Zn–Fe
100	39.06	0.43	0.49	0.48
101	43.26	0.47	0.55	0.56
102	54.27	0.60	0.74	0.65
110	70.05	0.79	0.89	0.80
112	82.08	0.73	1.08	0.93
201	86.57	0.70	0.76	0.75
202	94.82	0.70	0.88	0.79
203	109.16	1.05	1.25	1.10

Table 2. **Integral breadth of Zn–Ni coating diffraction lines (10° inclination beam)**

(*hkl*)	2θ	Integral breadth, rad
330	42.85	0.91
600	62.26	1.27
444	73.26	1.99
552	78.69	0.73
741	89.36	1.10
660	94.26	1.07

A decrease in crystalline perfection affects the surface reactivity and usually increases it. The bare Zn–Co surface seems to be more active than those of Zn and Zn–Fe, and this is why the amount of oxide phase formed during the initial corrosion stages was higher on this alloy. However, the resulting film on this sample was thinner but at the same time more protective. The coating microstructure most probably affected the oxide layer formation rate as well as their properties (crystallinity) and hence the corrosion resistance of these electrodeposits.

For Zn–Ni coatings, the values of the integral breadth of most diffraction lines were higher than for other coatings. Nevertheless, as Zn–Ni possessed a different crystal lattice symmetry than pure Zn and low-alloyed Zn coatings, it was unsuitable to compare these parameters. Even so, the surface activity in oxide film formation during the initial stages of corrosion for Zn–Ni samples was also higher, than for pure Zn and Zn–Fe surfaces. Thus, we can assume that Zn–Ni alloy, like Zn–Co, possesses a more distorted lattice than Zn and Zn–Fe.

CONCLUSIONS

Zn–Ni and Zn–Co coatings exhibited lower corrosion rates in HCO_3^--containing NaCl solution compared to those of Zn–Fe and Zn samples. Meanwhile, except the initial corrosion process stages, the amount of oxide phase formed as a corrosion product was higher for the coatings that possessed higher corrosion rates.

The corrosion process of electrodeposited Zn alloys was more uniform regarding the surface topography, while local corrosion attack was more pronounced for unalloyed Zn samples. During the corrosion process its surface became rougher, while for the alloys, especially Zn–Ni, the surface became smo-

other with respect to the initial state. Crystal shape modification (loss of the pyramidal shape) during the corrosion of Zn and low-alloyed Zn coatings took place.

The higher amount of crystallites with low-index plane orientation in Zn–Ni and Zn–Co coatings may be one of the reasons of their higher corrosion resistance.

The high surface activity of bare Zn–Co and Zn–Ni coatings in oxide film formation during the initial corrosion steps and the higher values of the integral breadth of almost all diffraction peaks of these specimens imply that these coating lattices possess a higher number of imperfections. Possibly, the structure of these electrodeposits favors oxide film formation with a higher corrosion resistance and at the same time is the reason for the differences detected in Zn and Zn alloy corrosion behaviour.

Received 02 June 2004
Accepted 22 June 2004

References

1. R. Ramanauskas, P. Quintana, L. Maldonado, R. Pomes and M. A. Pech-Canul, *Surf. Coat. Tech*., **92**, 16 (1997).
2. R. Ramanauskas, L. Muleshkova, L. Maldonado and P. Dobrovolskis, *Corros. Sci.*, **40**, 401 (1998).
3. R. Ramanauskas, *Appl. Surf. Sci*., **153**, 53 (1999).
4. G. Zhang, *Corrosion and Electrochemistry of Zinc*, Plenum Press, New York (1996).
5. M. E. Vela, G. Andreasen, S. G. Aziz, R C. Salvarezza and A. J. Arvia, *Electrochim. Acta*, **43**, 3 (1998).
6. R. Ramanauskas, M. A. Pech-Canul, P. Quintana, L. Maldonado and P. Bartolo-Perez, In: *Passivity and its Breakdown*, The Electrochem. Soc. Proc., Pennington, USA, **97–26**, 846 (1998).
7. L. Ph. Berube and G. L'Esperance, *J. Electrochem. Soc*., **136**, 2314 (1989).
8. R. Guo, F. Weinberg and D. Tromans, *Corrosion*, **51**, 356 (1995).
9. R. Ramanauskas, M. A. Pech-Canul and L. Diaz, In: Abstr. 3rd National Lithuanian Conference 'Chemistry 97', Vilnius, Lithuania, 51 (1997).
10. M. G. Fernandes and R. M. Latanision, *Physical Review B*, **47**, 11749 (1993).
11. P. A. Adcock, A. R. Ault and O. M. G. Newman, *J. Appl. Electrochem*., **15**, 865 (1985).
12. D. J. MacKinnon, J. M. Brannen and R. C. Kerby, *J. Appl. Electrochem*., **9**, 55 (1979).
13. H. Park and J. A. Szpunar, *Corros. Sci.*, **40**, 525 (1998).
14. R. F. Ashton and M. P. Hepworth, *Corrosion*, **24**, 50 (1968).
15. D. Abayarathna, E. B. Hale, T, J. O'Keefe, Y. M. Wang and D. Radovic, *Corros. Sci.*, **32**, 755 (1991).
16. F. Mansfeld and S. Gilman, *J. Electrochem. Soc*., **117**, 588 (1970).
17. S. R. Morrison, *Electrochemistry at Semiconductor and Oxidized Metal Electrodes*, Plenum Press, New York (1980).
18. Th. H. de Keijser, J. I. Langford, E. J. Mittemeijer and A. B. P. Vogels, *J. Appl. Cryst*., **15**, 308 (1982).
19. S. Enzo, G. Fagherazzi, A. Benedetti and J. Polizzi, *J. Appl. Cryst*., **21**, 536 (1988).
20. D. J. Balzar, *J. Appl. Cryst*., **25**, 559 (1992).
21. J. G. M. Van Berkum, R. Delhez, Th. H. de Keijser and E. J. Mittemeijer, *Acta Cryst.*, **A52**, 730 (1996).
22. B. D. Cullity, *Elements of X-Ray Diffraction*, 2nd ed., Addison-Wesley Reading, USA (1978).

Algirdas Selskis, Laima Gudavičiūtė, Ignas Valsiūnas, Rimantas Ramanauskas

Zn IR Zn LYDINIŲ GALVANINIŲ DANGŲ KOROZIJA: MORFOLOGINIAI IR STRUKTŪRINIAI POKYČIAI

S a n t r a u k a

Zn, Zn–Co (0,6%), Zn–Fe (0,4%) ir Zn–Ni (12%) galvaninių dangų korozinė elgsena buvo tirta HCO_3 ir NaCl terpėje. Korozijos proceso greičiai ir jo eigoje susidarančių oksidinių plėvelių savybės buvo nagrinėjamos ieškant koreliacijos su dangų mikrostruktūra. Atomo jėgos mikroskopija taikyta paviršiaus morfologiniams tyrimams bei šiurkštumo parametrų įvertinimui, rentgeno difrakciniai matavimai panaudoti dangų tekstūros pokyčiams bei metalo gardelės deformacijoms įvertinti. Daroma prielaida, kad oksidinė plėvelė turi didelę įtaką šių lydinių korozijos procesams. Didesnis paviršiaus aktyvumas, sąlygojamas gardelės defektingumo, nulemia geresnį Zn–Co ir Zn– Ni dangų korozinį atsparumą. Šios struktūrinės savybės įgalina sparčiau susiformuoti oksidinei plėvelei, o tai sumažina dangos korozijos greitį.